Quantifying regolith erosion rates with cosmogenic nuclides ^{10}Be and ^{26}Al in the McMurdo Dry Valleys, Antarctica

Daniel Morgan,[1,2] Jaakko Putkonen,[3] Greg Balco,[4] and John Stone[1]

[1]   The McMurdo Dry Valleys, Antarctica (MDV) are among the oldest landscapes on Earth, and some landforms there present an intriguing apparent contradiction such that millions of years old surface deposits maintain their meter-scale morphology despite the fact that measured erosion rates are 0.1–4 m Ma^{-1}. We analyzed the concentration of cosmic ray-produced ^{10}Be and ^{26}Al in quartz sands from regolith directly above and below two well-documented ash deposits in the MDV, the Arena Valley ash (^{40}Ar/^{39}Ar age of 4.33 Ma) and the Hart ash (K-Ar age of 3.9 Ma). Measured concentrations of ^{10}Be and ^{26}Al are significantly less than expected given the age of the in situ air fall ashes and are best interpreted as reflecting the degradation rate of the overlying sediments. The erosion rate of the material above the Arena Valley ash that best explains the observed isotope profiles is $3.5 \pm 0.41 \times 10^{-5}$ g cm^{-2} yr^{-1} (~0.19 m Ma^{-1}) for the past ~4 Ma. For the Hart ash, the erosion rate is $4.8 \pm 0.21 \times 10^{-4}$ g cm^{-2} yr^{-1} (~2.6 m Ma^{-1}) for the past ~1 Ma. The concentration profiles do not show signs of mixing, creep, or deflation caused by sublimation of ground ice. These results indicate that the slow, steady lowering of the surface without vertical mixing may allow landforms to maintain their meter-scale morphology even though they are actively eroding.

1. Introduction

[2]   Quantifying erosion rates is central to understanding how landscapes evolve through time and for discerning the linkages between landforms and the processes that shape them. The McMurdo Dry Valleys in Antarctica (MDV) have a unique hyperarid, cold, polar desert climate and are among the oldest landscapes on Earth [e.g., *Denton et al.*, 1993; *Schäfer et al.*, 1999], which makes geomorphologists wonder: how low can erosion rates be? The preservation of ash deposits up to 15 Ma old at the present-day surface has been interpreted as indicating that the climate in the MDV has remained cold and dry for millions of years and that very little landscape evolution has occurred over this time [*Denton et al.*, 1993; *Hall et al.*, 1993; *Marchant et al.*, 1993a, 1993b; *Marchant and Denton*, 1996; *Marchant et al.*, 1996; *Lewis et al.*, 2007; *Marchant and Head*, 2007]. Supporting the notion that the MDV are a relict landscape where degradation rates are vanishingly small is the observation that many glacial moraines and landslide deposits have maintained their meter-scale morphology even though they are millions of

years old [e.g., *Denton et al.*, 1984; *Marchant et al.*, 1993a; *Sugden et al.*, 1995; *Lewis et al.*, 2007] and the Antarctic ice sheets have fluctuated significantly over this time period [*Naish et al.*, 2009].

[3]   Many surface deposits in the MDV have sharp breaks in slope, visible at the crests of glacial moraines and where the toes of landslides and moraines abruptly contact the surrounding hillslopes, which suggests that diffusive-like geomorphic process are not active in this environment. Our general understanding of regolith degradation is that geomorphic processes act to smooth topography over time, and is based on studies of fault scarps, hillslopes, and moraines from the midlatitudes [*Nash*, 1980; *Hanks et al.*, 1984; *Fernandes and Dietrich*, 1997; *Hanks*, 2000; *Putkonen and O'Neal*, 2006]. In the MDV, many surface deposits have maintained their sharp morphology for millions of years even though measured bedrock and regolith erosion rates in the MDV range from 0.1 to 4 m Ma^{-1} [*Summerfield et al.*, 1999; *Putkonen et al.*, 2008]. Even slow erosion rates such as these should be sufficient to alter the meter-scale morphology of unconsolidated deposits after a few million years. This observation presents an apparent contradiction between measured erosion rates and the meter-scale morphology of these deposits and also challenges our understanding of how unconsolidated deposits evolve through time.

[4]   In this paper we use the term regolith to mean the loose, incoherent mantle of rock fragments, soil, glacial drift, blown sand, etc., that rests upon solid bedrock [*Whitten and Brooks*, 1987]. We will use this term in this paper when the source of unconsolidated material in the MDV is not known, and

---

[1]Department of Earth and Space Sciences, University of Washington, Seattle, Washington, USA.
[2]Now at Department of Earth and Environmental Sciences, Vanderbilt University, Nashville, Tennessee, USA.
[3]Department of Geology and Geological Engineering, University of North Dakota, Grand Forks, North Dakota, USA.
[4]Berkeley Geochronology Center, Berkeley, California, USA.
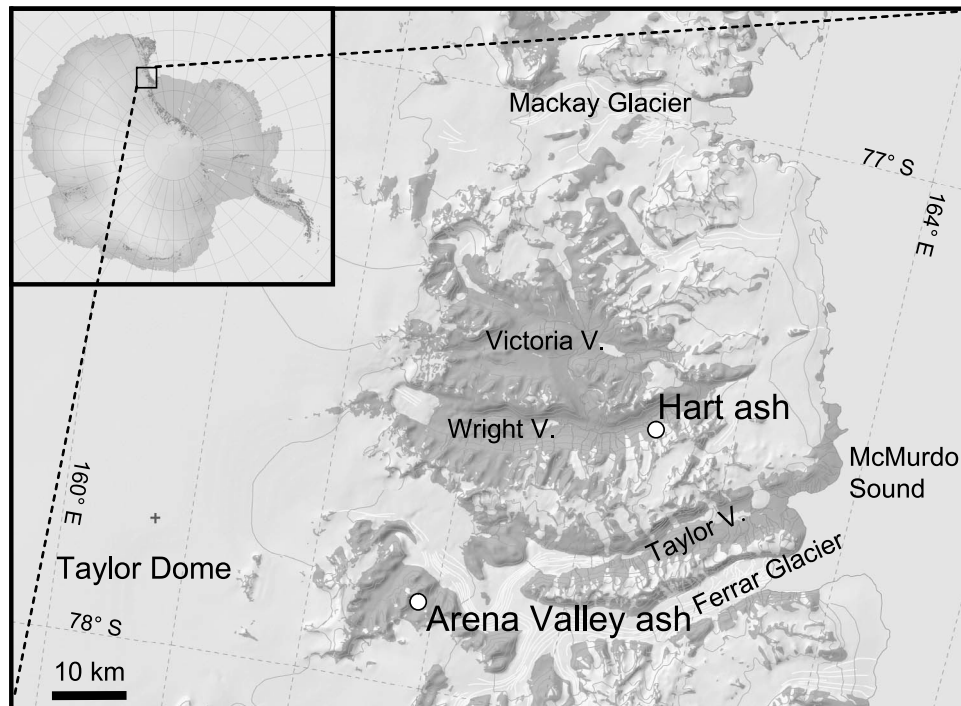
Figure 1. Map of Antarctica (inset) and the McMurdo Dry Valleys. The white circles show the location of the two ash deposits studied in this paper.

therefore terms like colluvium or eolian deposit may not be appropriate. We will use the term colluvium to describe units that have been defined as such by previous researchers. Additionally, we will use the term degradation to mean the general lowering of the Earth's surface, regardless of process [*Whitten and Brooks*, 1987].

[5] The objective of this study is to quantify subaerial regolith degradation rates in a cold polar desert and to explore the apparent contradiction between the measured bedrock and regolith erosion rates and the preservation of surface deposits for millions of years in the MDV. To do this, we will use the concentration of cosmogenic nuclides ^{10}Be and ^{26}Al in quartz sands from above and below two well-documented air fall ash deposits to examine the postdepositional geologic history of these surfaces. These deposits are the Arena Valley ash in Arena Valley (^{40}Ar/^{39}Ar age of 4.33 ± 0.07 Ma [*Marchant et al.*, 1993a]) and the Hart ash in Wright Valley (K-Ar age of 3.9 ± 0.3 Ma [*Hall et al.*, 1993]). Because we know the age of these ashes, we can use the concentration of cosmogenic nuclides to examine specific questions about how these surfaces have evolved since they were deposited, including the exposure duration, erosion rate, vertical mixing, and burial history. This has allowed us to investigate the apparent contradiction between the preservation of meter-scale surface features for up to ~15 Ma and erosion rates at the ~m Ma^{-1} scale. Furthermore, determining the rates at which regolith degrades in the MDV will advance our understanding of landscape evolution in cold and hyperarid environments.

2. Field Area and Sample Sites

[6] Located between the East Antarctic Ice Sheet and the Ross Sea (Figure 1), the McMurdo Dry Valleys are free of ice because ice sublimation rates are equal to or higher than snow precipitation rates [*MacClune et al.*, 2003] and because glacial ice from the Taylor dome is diverted around the MDV and through the Ferrar and Mackay Glaciers [*Chinn*, 1990]. The MDV have a hyperarid, cold, polar desert climate. The annual precipitation, as measured at Lake Vanda in Wright Valley (93 m above sea level, asl), is less than 100 mm water equivalent [*Fountain et al.*, 1999]. Though running meltwater is common in the lower valleys (~200 m asl) during the austral summer, it is rarely observed in the upper valleys (>1000 m asl). The mean annual temperature on the valley floor of Wright Valley is −17.7°C [*Doran et al.*, 2002], and in Beacon Valley (which is adjacent to Arena Valley) it is −24°C [*Putkonen et al.*, 2003].

[7] Mean annual temperature and precipitation in the MDV follow a strong east–west climate gradient, which is related to the elevation, distance from the coast, and the exposure of the landscape to katabatic winds [*Fountain et al.*, 1999; *Doran et al.*, 2002]. Many researchers have classified microclimate zones in the MDV [e.g., *Campbell and Claridge*, 1969, 1987, 2006; *Bockheim*, 2002], and *Marchant and Denton* [1996] (later expanded by *Marchant and Head* [2007]) defined these zones by the characteristic equilibrium geomorphic landforms that would form in each microclimate. These zones are the stable upland zone, the inland mixed zone, and the coastal thaw zone. The sample sites are located in two different microclimate zones, which will allow us to explore the potential role that microclimate may play on regolith degradation rates. The Arena Valley ash is found in the stable upland zone (mean annual temperature, −22°C) and the Hart ash is found in the inland mixed zone (mean annual temperature, −18°C).
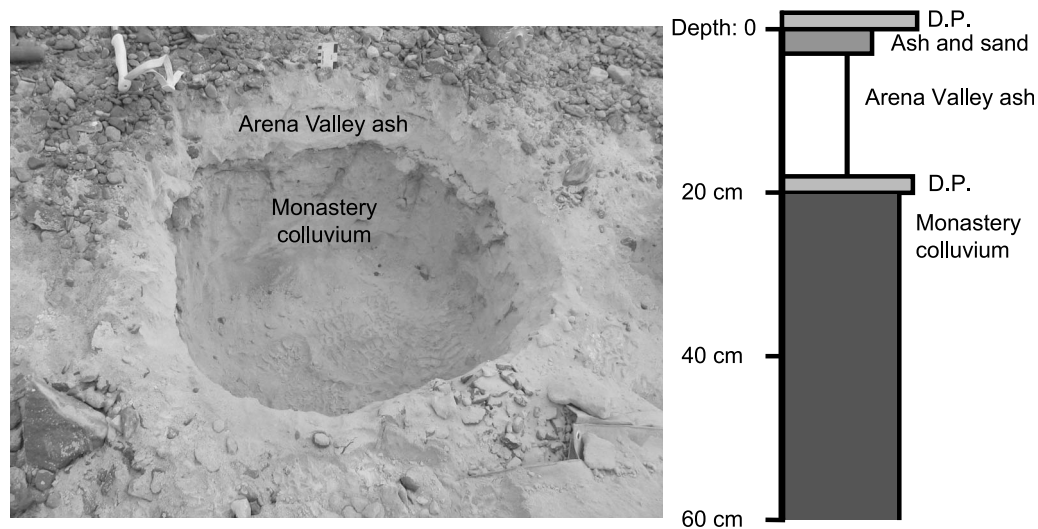
Figure 2. The Arena Valley ash and the stratigraphy of the site (04-AV-Pit 4). Widths of the stratigraphic columns represent relatively larger average sediment grain size of the unit. D.P. indicates a desert pavement. At this site, the Arena Valley ash is 15 cm thick, beginning 3 cm below the desert pavement that makes the current surface. The Arena Valley ash has an ^{40}Ar/^{39}Ar age of 4.33 Ma [*Marchant et al.*, 1993a] and rests on a desert pavement that caps the Monastery colluvium.

[8] Because the interpretation of the cosmogenic nuclide concentrations is founded in the geologic setting, we must have a firm understanding of the geologic setting that these samples have come from. We use the geologic setting to describe and constrain the events that have occurred at these sites, and then we can use the cosmogenic nuclides to explore when the events occurred and how fast these processes operate. The following sections will provide a detailed description of the geologic events that occurred at each site, from which we will build our interpretation of the results.

2.1. The Arena Valley Ash

[9] The Arena Valley ash was first described by *Marchant et al.* [1993c] and was later described in more detail by *Marchant et al.* [1993a]. As described by *Marchant et al.* [1993a], the ash is about 25 cm thick, underlies the modern desert pavement, and was deposited on a desert pavement that armors the Monastery colluvium. *Marchant et al.* [1993a] described the deposit as having a basal unit that is 0.5– 1.0 cm thick that lacks nonvolcanic contaminants and lies in sharp stratigraphic contact with the underlying desert pavement. On the basis of these characteristics, *Marchant et al.* [1993a] interpreted the Arena Valley ash as an in situ air fall ash. The ^{40}Ar/^{39}Ar age of sanidine in the ash is 4.33 ± 0.07 Ma.

[10] Following the description of the site in the work of *Marchant et al.* [1993a], we found the Arena Valley ash near the foot of the slope of the main tributary valley in west central Arena Valley (04-AV-Pit 4: 77.86378°S, 160.84510°E, and 1364 m). We measured depth down from the surface beginning at the bottom of the modern desert pavement and found that the top 3 cm was a mixture of colluvial sands and some ash, 3–18 cm was entirely ash, 18–20 cm was the buried desert pavement, and below 20 cm was the Monastery colluvium (Figure 2). Visual inspection of the basal unit of the ash under magnification showed that delicate glass shards and spires remained intact, suggesting that the ash was an air fall ash.

[11] On the basis of the geologic description of the Arena Valley ash pit, the following geologic events occurred at the sample site. Before the ash was emplaced, a colluvium layer with a well-developed desert pavement, consisting of sandstone and dolerite gravel, was at the surface. Because this desert pavement caps the colluvium abruptly and is not underlain by a layer of eolian sands, which would indicate inflation, the pavement likely formed as the result of deflation of the underlying colluvium. Thus, the desert pavement that underlies the Arena Valley ash indicates that the surface was undergoing erosion before the ash was deposited. At 4.33 Ma, the Arena Valley ash was deposited on this desert pavement. The contact between the buried desert pavement and the Arena Valley ash was found to be nearly parallel to the slope and did not appear to be deformed by any vertical mixing in the 4.33 Ma since the ash was deposited.

[12] Today, the Arena Valley ash is capped by a second desert pavement. This pavement consists of a coarse lag deposit of dolerite and sandstone gravel and cobbles. Though the upper 3 cm of ash contain some nonvolcanic contaminants, there are no massive deposits of eolian sands that would indicate inflation. Thus, the desert pavement that caps the Arena Valley ash also likely indicates erosion. What is not clear from the geologic setting is the source of the material that created this upper desert pavement. It is possible that a thicker layer of colluvium once covered the ash, that the ash layer itself was thicker, that the modern desert pavement represents a thin layer of actively mobile material at the surface, or that a combination of these possibilities at various times in the 4.33 Ma since the ash was deposited. The unknown parameters that we hope to address at this site include the erosion rates before and after the ash was deposited, the amount of burial by colluvium that may have covered the ash, and the potential for cold-based ice to have covered the site from cosmic rays and preserved it from erosion.
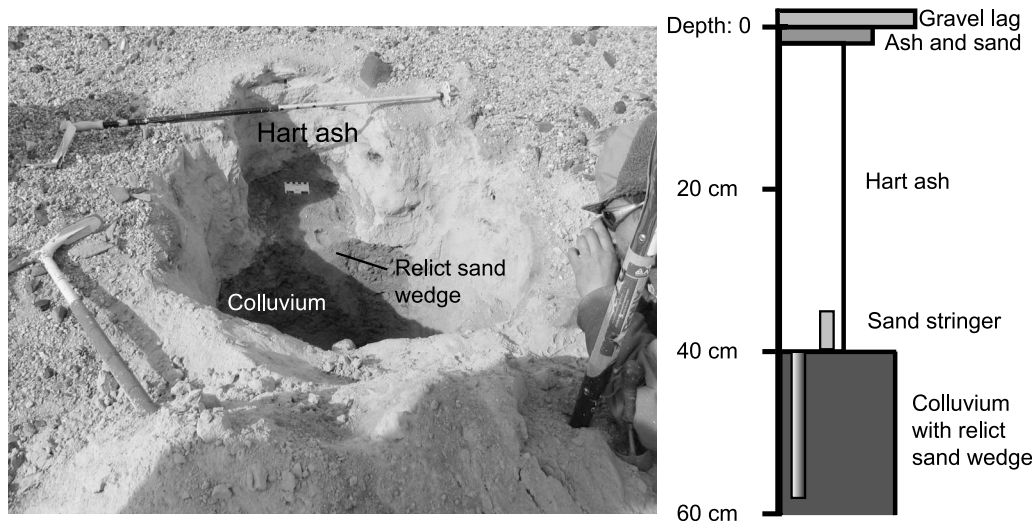
Figure 3. The Hart ash and the stratigraphy of the site (04-LWV-Pit 25). Widths of the stratigraphic columns represent relatively larger average grain size of the unit. At this site, the Hart ash is 38 cm thick, beginning 2 cm below the gravel lag that makes the current surface. The Hart ash has a K-Ar age of 3.9 Ma [*Hall et al.*, 1993] and rests on a colluvium layer that contains a relict sand wedge. The sand wedge ends abruptly at the contact between the ash and the colluvium and does not penetrate the ash, indicating that any cryoturbation that formed the sand wedge predates the deposition of the ash. Sand stringers do extend into the ash a few centimeters, indicating that the ash and colluvium underwent some soft sediment deformation.

2.2. The Hart Ash

[13] The Hart ash in Lower Wright Valley was first described by *Hall et al.* [1993] and was found at three different localities. As described by *Hall et al.* [1993], the ash is usually 30–40 cm thick, the upper 20–30 cm are usually disturbed and contain a few sand stringers and/or clasts, but the lower units are pure ash, undisturbed, and have a sharp basal contact with the underlying colluvium. In some excavations, *Hall et al.* [1993] found that the ash was deposited on a poorly developed desert pavement. Because the thinner edges of the ash deposits have been reworked, *Hall et al.* [1993] suggest that the ash may have been overridden by westward flowing ice after its deposition. On the basis of the sharp basal contact with the underlying colluvium and the undisturbed basal layers of the ash, *Hall et al.* [1993] interpreted the ash as a primary deposit, and glass in the ash has a K-Ar age of 3.9 ± 0.3 Ma. The largest deposit of the Hart ash (150 m × 85 m) found by *Hall et al.* [1993] was located between the Hart and Goodspeed glaciers at an elevation of 378 m.

[14] Following the description of the most extensive deposit in the work of *Hall et al.* [1993], we found the Hart ash between the Hart and Goodspeed glaciers in Lower Wright Valley (04-LWV-Pit 25: 77.49587°S, 162.37390°E, and 386 m). The sample site (Figure 3) is capped by a gravel lag that consists of granitoid clasts of gravel that are mobile during high wind events, as evidenced by the gravel ripples observed in the surrounding area. The ash generally began 1–2 cm below this gravel lag, but in places a thin (<10 cm) colluvium layer was above the ash. Where we sampled the sediment, we found that the upper 2 cm of the soil was a mixture of sand and ash and that pure ash began 2 cm below the gravel lag and reached a depth of 40 cm. Below the ash was a strongly discolored (most likely oxidized) colluvium

layer. Though this colluvium layer was oxidized, it lacked salt pans, which would indicate either a lack of moisture delivering salt to this site, or that the colluvial surface was eroding before the ash was deposited. At this site, we found a relict sand wedge that terminated abruptly at the colluvium-ash contact, suggesting that thermal contraction and infilling of the cracks with sand predated the deposition of the ash. Additionally, we found a few sand stringers that cut into the ash, suggesting that some soft sediment deformation occurred during the deposition of the ash. For cosmogenic nuclide analysis, we used samples from the colluvium below the ash and not the sand wedge or the sand stringers. Visual inspection of the basal unit of the ash under magnification found delicate glass shards and spires, suggesting that the ash was an air fall ash.

[15] The geologic description of the Hart ash site indicates that the following geologic events occurred at this site. The presence of a relict sand wedge in the colluvium underlying the Hart ash implies that the colluvium was subject to cryoturbation before the ash was deposited, and we would expect some vertical mixing of the sediment as a result. The relict sand wedge terminates abruptly at the contact with the Hart ash, which implies that there is an erosional surface at the top of the colluvium and that the site experienced erosion before the ash was deposited. At 3.9 Ma, the Hart ash was deposited on this erosional surface. The Hart ash is now capped by a gravel lag. Though the upper 2 cm of ash contains nonvolcanic contaminants, there are no massive deposits of eolian sands, which would indicate inflation. Thus, the gravel lag that caps the Hart ash also likely indicates erosion of the surface, though the presence of nonvolcanic sediments in the upper few centimeters of the ash does indicate some infiltration of sediments. *Hall et al.* [1993] suggest that the site may have been covered by weakly erosive cold-based ice and the sample site is above the 300 m elevation limit of fjord

Table 1. Sample and Isotope Data[a]

Sample ID	Depth in Soil (cm)	Soil Density (g cm^{-3})	Effective Shielding Mass (g cm^{-2})	^{10}Be $10^6 \pm 1$ Std Uncertainty (atoms g$^{-1}_{quartz}$)	^{26}Al $10^6 \pm 1$ Std Uncertainty (atoms g$^{-1}_{quartz}$)
			04-AV-Pit 4: Arena Valley Ash		
04-AV-Pit 4 0-1	0–1	1.78	0.907	11.4 ± 0.322	61.6 ± 2.07
Arena Valley ash	3–18	1.02	n.m.	n.m.	n.m.
04-AV-Pit 4 20–23	20–23	1.84	27.0	23.7 ± 0.994	88.6 ± 4.34
04-AV-Pit 4 30–33	30–33	1.83	45.1	20.6 ± 0.970	79.4 ± 2.59
04-AV-Pit 4 40–43	40–43	1.83	63.3	n.m.	74.6 ± 2.82
04-AV-Pit 4 50–53	50–53	1.80	81.4	15.0 ± 0.477	64.5 ± 2.80
04-AV-Pit 4 60–63	60–63	1.81	99.6	16.3 ± 1.41	54.7 ± 2.72
			04-LWV-Pit 25: Hart Ash		
04-LWV-Pit 25 0–2	0–2	1.32	1.31	n.m.	15.4 ± 0.835
Hart ash	2–40	1.01	n.m.	n.m.	n.m.
04-LWV-Pit 25 45–48	45–48	1.76	52.9	2.60 ± 0.0757	10.5 ± 0.526
04-LWV-Pit 25 55–58	55–58	1.76	71.0	2.14 ± 0.0815	7.80 ± 0.406
04-LWV-Pit 25 65–68	65–68	1.81	89.1	2.16 ± 0.110	n.m.
04-LWV-Pit 25 77–80	77–80	1.91	111	1.99 ± 0.0948	5.72 ± 0.567

[a]n.m. indicates that no measurements are available for this sample.

deposits found in Wright Valley [*Hall et al.*, 1993; *Prentice and Krusic*, 2005], which suggests that the site may have been buried by ice, but was probably not buried by water. The unknowns at this site are the erosion rate after the ash was deposited, the extent and timing of the cryoturbation and erosion that predate the ash emplacement, and the possibility that cold-based ice covered this site and shielded the sediments from cosmic rays and erosion.

[16] There are a number of similarities in the geologic setting of the two ash deposits studied, but there are also a few important differences. Both ash deposits are primary, air fall ashes that have a sharp stratigraphic contact with the underlying colluvium. The Arena Valley ash rests upon a well-developed desert pavement that consists of sandstone and dolerite clasts, whereas the Hart ash lies directly upon an eroded colluvium layer that is not capped by any sort of pavement or lag deposit. The desert pavement that the Arena Valley ash lies on remains nearly slope parallel and does not show any indication that it has been deformed or vertically mixed since the ash was deposited. Though the colluvium that underlies the Hart ash contains a relict sand wedge, this sand wedge terminates abruptly at the contact of the ash, indicating that cryoturbation and vertical mixing were likely active before the ash was deposited, but not since. The material that caps each ash is different, with the Arena Valley ash being capped by a well-developed desert pavement consisting of sandstone and dolerite ventifacts. The Hart ash is capped by granitoid gravels. Finally, following the microclimate zones defined by *Marchant and Head* [2007], the Arena Valley ash is located in the stable upland zone whereas the Hart ash is located in the inland mixed zone. Because of the climatic differences between these two zones, we can expect that rates of geomorphic processes may differ between these two sites.

3. Methods

3.1. Sample Collection and Processing

[17] In the field, we collected a series of bulk sediment samples from ~1 m deep hand-dug soil pits. At both sample sites, we collected a sediment sample from just below the modern desert pavement, a series of samples of the ash itself, and a series of samples from the colluvium that underlies the

ash. We measured the density of the colluvium and the ash by packing the sediment samples into a container of known volume. This packing method was repeated multiple times for each sample to obtain the range and mean of the sediment densities. The sample depths and densities are found in Table 1.

[18] To extract quartz from the sediment, we dry sieved the samples and subsampled the 0.3–0.5 mm size fraction. To remove pyroxene derived from the local dolerite, we used a heavy liquid separation, and the quartz was purified by repeated etching in 2% HF. We extracted beryllium and aluminum using standard methods [*Stone*, 2004] and measured ^{10}Be/^{9}Be and ^{27}Al/^{26}Al isotope ratios at the PRIME lab at Purdue University in West Lafayette, IN. The combined carrier and process blanks contained $1.67 \pm 0.462 \times 10^5$ atoms ^{10}Be and $0 \pm 2.04 \times 10^5$ atoms ^{26}Al. These are always less than 0.9% of the measured ^{10}Be atoms and 0.45% of the measured ^{26}Al atoms. The beryllium measurements were originally standardized to the ICN standard, and we have restandardized them to the 07KNSTD [*Nishiizumi et al.*, 2007]. For aluminum, the isotope ratios were referenced to the *Nishiizumi* [2004] standard. We determined the ^{10}Be and ^{26}Al production rates at the sample sites by using the rates of *Stone* [2000]. ^{10}Be production rates were further reduced by a factor of 1.106 following *Nishiizumi et al.* [2007]. For the Arena Valley ash (04-AV-Pit 4) the topographic shielding factor for the site is 0.98, and the resulting surface production rates are 19.4 ± 1.3 atoms g^{-1} yr^{-1} for ^{10}Be and 131.2 ± 7.3 atoms g^{-1} yr^{-1} for ^{26}Al. For the Hart ash (04-LWV-Pit 25), the topographic shielding factor for the site is 0.99 and the resulting surface production rates are 8.21 ± 0.56 atoms g^{-1} yr^{-1} for ^{10}Be and 55.7 ± 3.1 atoms g^{-1} yr^{-1} for ^{26}Al. The nuclide concentration data are given in Table 1.

3.2. Exposure Model

[19] The general concept for analyzing the cosmogenic nuclide measurements is to use the local geologic and geomorphic context to determine what happened geologically. We construct an exposure model to describe these geologic events and use the ^{10}Be and ^{26}Al concentrations to determine when and how fast the geologic events occurred. This method is built upon the fact that the measured concentration

of cosmogenic nuclides is a function of the exposure duration and the production rate of these isotopes, which is itself dependent upon the shielding mass history of the samples [*Lal*, 1991]. In this framework, erosion can be viewed as the removal of shielding mass, deposition is the addition of shielding mass, and any geomorphic process that can be described as a change in depth through time can be directly turned into an exposure model that mathematically expresses how the shielding of a sample changed through time. This type of analysis is particularly well-suited to these specific sample sites because the ages of the ashes are known, which allows us to further explore specific questions about how these sites have been exposed, such as, has the regolith remained undisturbed since the deposition of the ash, has it been subjected to surface degradation, vertical mixing of the deposit due to an activity like cryoturbation, downslope creep processes, and any combination of these processes. Additionally, the sites could have been covered by weakly erosive, cold-based ice sometime after the ash was deposited, which would have strongly affected the resulting cosmogenic isotope concentrations of the underlying regolith. The key to this method is that all of these geologic possibilities would result in a change in the shielding of the samples, which would result in a change in the final concentration of cosmogenic nuclides of the samples. By comparing the measured concentrations to the theoretical concentrations from different exposure models, we can test the validity of various exposure models.

[20] The production of ^{10}Be and ^{26}Al at less than 1 m depth is almost entirely by spallation [*Gosse and Phillips*, 2001], which means that the production rate of ^{10}Be and ^{26}Al below the surface can be described by:

$$P_i(z) = P_i(0) \cdot e^{-z/\Lambda}, \quad (1)$$

where the subscript i indicates the nuclide of interest (either ^{10}Be or ^{26}Al), $P_i(0)$ is the surface production rate of nuclide i and has units of atoms g^{-1} yr^{-1}, z is the effective shielding mass of the sample and has units of g cm^{-2}, and Λ is the attenuation length, which is taken to be 150 g cm^{-2} in Antarctica (see *Lal* [1991] and *Gosse and Phillips* [2001] for a discussion of Λ). The shielding mass is the shielding provided by the overlying sediments for each sample, which is related to the depth of the sample below the surface and cumulative density of the overlying material. The effective shielding mass is the point in the sample where the isotope production rate (for either ^{10}Be or ^{26}Al) is equal to the average isotope production rate through the thickness of the sample.

[21] The production and decay of nuclide i in sample j is governed by [*Lal*, 1991]:

$$\frac{dN_{i,j}}{dt} = P_i(z_j(t)) - N_{i,j}\lambda_i, \quad (2)$$

where N is the nuclide concentration that we have measured, P is the production rate at the sample site and is dependent on the shielding mass z (g cm^{-2}) of the sample, λ is the decay constant (yr^{-1}) for nuclide i, and the subscript j indicates the sample number. In this study, we have used decay constants of $\lambda_{10} = 5.1 \times 10^{-7}$ yr^{-1} for ^{10}Be [*Nishiizumi et al.*, 2007] and $\lambda_{26} = 9.78 \times 10^{-7}$ yr^{-1} for ^{26}Al [*Nishiizumi*, 2004].

[22] An exposure model is a function, $z_j(t)$, that describes how the shielding of a sample changes through time, which depends on unknown parameters like the rates of geologic processes and the length of time that these processes occurred over. The exposure model is used to calculate nuclide concentrations for a set of the unknown parameters that we compare to the measured abundances. To assess the quality of fit between an exposure model and the measured cosmogenic nuclide concentrations, we used an error-weighted, least squares method. The best fit values for the unknowns in the exposure model are those that minimize the difference between the modeled and measured concentrations.

3.2.1. Steady Erosion Exposure Model

[23] If we disregard soil mixing, the process of steady exposure and steady degradation since the deposition of the ash would result in a nuclide concentration–depth relationship according to the simple exposure age equation of *Lal* [1991]. Additionally, we must include any inherited nuclides from before the ash was deposited that might remain in the samples. The concentration of nuclides that we expect is the sum of the inherited nuclides plus those that accumulated after the deposition of the ash:

$$N_{i,j}(N_{i,\text{inh}}, \varepsilon, t_{\text{ash}}) = N_{i,\text{inh}} + \frac{P_i(z_j)}{(\lambda_i + {}^{\varepsilon}/_\Lambda)} \cdot (1 - e^{-(\lambda_i + {}^{\varepsilon}/_\Lambda) \cdot t_{\text{ash}}}), \quad (3)$$

where $N_{i,\text{inh}}$ is the concentration of nuclide i inherited from before the ash was deposited that remains in the sediment today, t_{ash} is the depositional age of the ash, and ε is the erosion rate in g cm^{-2} yr^{-1} after the ash is deposited. This argument roughly follows the one in the work of *Balco et al.* [2005a, 2005b] for till and *Putkonen et al.* [2008] for regolith. Equation (3) depends on two unknown parameters, $N_{i,\text{inh}}$ and ε, and we have at least three measurements of each nuclide at each pit, so we can uniquely determine the unknowns.

[24] Equation (3) assumes that the inherited nuclides from before the ash was deposited are the same at all depths in the pit, and this would only be the case if the colluvium was well mixed before the ash was deposited. Additionally, we can test if the inherited nuclides record erosion before the ash was deposited without any vertical mixing. In this case, the inherited nuclides would fit an exponential profile that decreases exponentially with depth. If we assume that a steadily eroding colluvium with no vertical mixing had reached equilibrium with an erosion rate before the ash was deposited, we can modify equation (3) for an inherited nuclide profile that will fit an exponential profile that has subsequently decayed in the intervening years, and the erosion rate after the ash was deposited, we get:

$$N_{i,j}(\varepsilon_1, \varepsilon_2, t_{\text{ash}}) = \frac{P_i(z_j)}{(\lambda_i + {}^{\varepsilon_1}/_\Lambda)} \cdot e^{-(\lambda_i) \cdot t_{\text{ash}}} + \frac{P_i(z_j)}{(\lambda_i + {}^{\varepsilon_2}/_\Lambda)}$$
$$\cdot \left(1 - e^{-(\lambda_i + {}^{\varepsilon_2}/_\Lambda) \cdot t_{\text{ash}}}\right), \quad (4)$$

where ε_1 is the erosion rate before the ash is deposited and ε_2 is the erosion rate after the ash is deposited, and the erosion rates have units in g cm^{-2} yr^{-1}. Because the age of the ash is known and we have at least three pairs of nuclide concentration measurements at each site, we can solve equation (4) for the two unknown erosion rates.

3.2.2. Burial Exposure Model

[25] *Hall et al.* [1993] suggest that the Hart ash may have been buried by ice for a period of time so we need to address the possibility of burial in an exposure model. We can test for the possibility of burial by ice by building an exposure model with three time periods: (1) a steadily eroding surface after the ash is emplaced, (2) a period of burial by ice, and (3) a steadily eroding surface after the ice recedes. The total length of time of these three periods is the age of the ash. The concentration of cosmogenic nuclides that we expect in this case is dependent on four unknowns: ε_1 and t_1 (the erosion rate and the time period after the ash but before the burial by ice, respectively), t_b (the length of time the sediment was buried), and ε_2 (the erosion rate after the period of burial). The length of time that the sediment is exposed after any burial by ice (t_2) is set by the age of the ash because the age of the ash must be equal to the three periods of exposure. The concentration of nuclides that we expect from this scenario is:

$$
N_{i,j}(\varepsilon_1, \varepsilon_2, t_1, t_b) = \frac{P_i(z_j)}{(\lambda_i + \varepsilon_1/\Lambda)} \cdot \left(1 - e^{-(\lambda_i + \varepsilon_1/\Lambda)\cdot t_1}\right)
$$
$$
\cdot\, e^{-(\lambda_i)\cdot t_b} \cdot e^{-(\lambda_i)\cdot t_2} + \frac{P_i(z_j)}{(\lambda_i + \varepsilon_2/\Lambda)}
$$
$$
\cdot \left(1 - e^{-(\lambda_i + \varepsilon_2/\Lambda)\cdot t_2}\right). \tag{5}
$$

Additionally, we can consider inherited nuclides from before the emplacement of the ash in this exposure model following the methods described for equations (3) and (4) above.

3.2.3. Time Period of Measurements

[26] Because ^{10}Be and ^{26}Al are radiogenic nuclides, eventually an equilibrium will be reached between their production and decay. Additionally, erosion results in the loss of nuclides, which lowers the amount of time that it takes for the nuclide concentration to reach equilibrium between production and decay [*Gillespie and Bierman*, 1995]. The period of time that it takes cosmogenic nuclide concentrations to reach equilibrium with an erosion rate is controlled by the effective half life:

$$
\tau_{1/2,e} = \frac{\ln(2)}{(\lambda_i + \varepsilon/\Lambda)}, \tag{6}
$$

where ε is the erosion rate of the overlying regolith. After a several effective half-lives have passed, the ^{10}Be and ^{26}Al will have reached equilibrium with steady erosion, which limits the amount of time that the measurements record. Furthermore, changes in the erosion rate that are on much shorter time scales than the effective half-life will cause only small variations in the nuclide concentrations relative to the long-term erosional equilibrium concentration value [*Balco and Shuster*, 2009]. This means that if the effective half life is on the order of 10^5–10^6 years, then even changes in the erosion rate on the order of 10^4 years will not significantly affect the measured nuclide concentration. Even though erosion rates are not likely to be steady over 10^5–10^6 years, if erosion rates are low and the effective half life is long, then the measured nuclide concentrations will reflect the long-term average erosion rate over these time scales.

3.2.4. Error Analysis

[27] To determine the uncertainties for these results, we carried out a 10,000 run Monte Carlo simulation that took into account uncertainties in the measured nuclide concentrations. This method is described in detail by *Balco et al.* [2005b] and assumes that the measured nuclide concentrations are a Gaussian distribution with the 1 sigma errors reported in Table 1. Each run in the Monte Carlo simulation takes a random value for each data point from its Gaussian distribution and finds the best fit parameters to this set of data points. This exercise yields a histogram of possible solutions for the unknowns in the exposure models, from which we report the 68% confidence interval as the error of the best fit parameters.

4. Results

4.1. The Arena Valley Ash

[28] On the basis of the geologic description of the site and the observations of *Marchant et al.* [1993a] that the original amount of ash at the site was likely larger than is presently found there, we expect that the nuclide concentrations in the Monastery colluvium below the ash would reflect the surface degradation rate. Indeed, the cosmogenic nuclide concentrations below the Arena Ash are not consistent with an exposed, noneroding surface since the deposition of the ash. If we were to ignore surface erosion, the concentrations of ^{10}Be and ^{26}Al would yield an exposure age of the Monastery colluvium below the ash of only ~2 Ma, which cannot be true because it is overlain by a 4.33 Ma ash deposit. Thus, the cosmogenic nuclide concentrations below the ash either reflect the degradation rate at this site or burial.

[29] Following the geologic description of the site, we fit equation (4) to the nuclide measurements, which includes erosion before and after the ash emplacement, and no vertical mixing of the sediment, which is consistent with the observation that buried desert pavement remains slope parallel and in sharp contact with both the overlying and underlying sediments. This results in an erosion rate before the ash was deposited of $1.0 \pm 0.40 \times 10^{-4}$ g cm^{-2} yr^{-1} and that after the emplacement of the ash the erosion rate was $3.5 \pm 0.41 \times 10^{-5}$ g cm^{-2} yr^{-1}. These rates fit the measurements with a reduced chi square value of 1.3 for all nine data points (Figure 4a). We can test if the site was experiencing vertical mixing before the ash was deposited by fitting equation (3) to the data, but the fit for this exposure model (reduced chi square value of 1.7, Table 2) is not as good as it is for equation (4). Contour plots of the chi square fits for these exposure models are shown in Appendix A.

[30] The fact that the ^{10}Be and ^{26}Al measurements fit equation (4) well means that no vertical mixing of the soil has occurred in the period of time that these measurements record, which is controlled by the effective half life of the nuclides. The effect of vertical mixing on the measured nuclide concentrations would be to evenly distribute the concentrations as the sediment becomes well mixed. Because the measured concentrations decrease monotonically with depth and are fully captured by the simple exponential function in equation (4), vertical mixing has not been active at this site in the time period that these measurements record. For an erosion rate of 3.5×10^{-5} g cm^{-2} yr^{-1}, one effective half life of ^{10}Be is ~1 Ma and is ~0.6 Ma for ^{26}Al. Thus, these measurements indicate that steady erosion at a rate of 3.5×10^{-5} g cm^{-2} yr^{-1} has been occurring for the past ~4 Ma.

[31] Additionally, these results show that the site has not been buried and shielded from cosmic rays for the past ~4 Ma. Figure 4b shows the measured nuclide concentrations plotted on the Klein-Nishiizumi two-isotope diagram, which has been adjusted for the production rate of the nuclides at each sample depth. The general interpretation of this diagram is that cosmogenic nuclide concentrations that reflect only surface exposure plot on the upper line, concentrations that reflect erosion plot on the lower line, and concentrations that reflect a more complicated exposure history, such as burial or inheritance, plot below these lines. For each sample that we have of the concentrations of both ^{10}Be and ^{26}Al, the measurements are shown as black circles with ellipses around them representing the 1 sigma error envelopes. The black

circles and gray boxes in Figure 4 show the results of a Monte Carlo simulation that divides the nuclide concentrations into pre- and post-ash components following equation (4). Though the measured nuclide concentrations suggest that the site may have been buried by separating them into pre- and post-ash components, we can explain the measured concentrations as the sum of two erosional histories.

[32] The results from fitting equation (4) to the measurements suggest that the erosion rate before the ash was higher than after the ash was deposited. This is also illustrated in Figure 4b by the fact that the pre-ash concentrations plot farther to the left on the steady erosion line than the post-ash concentrations. However, the effective half-life of the nuclides suggests that the measurements only record what has
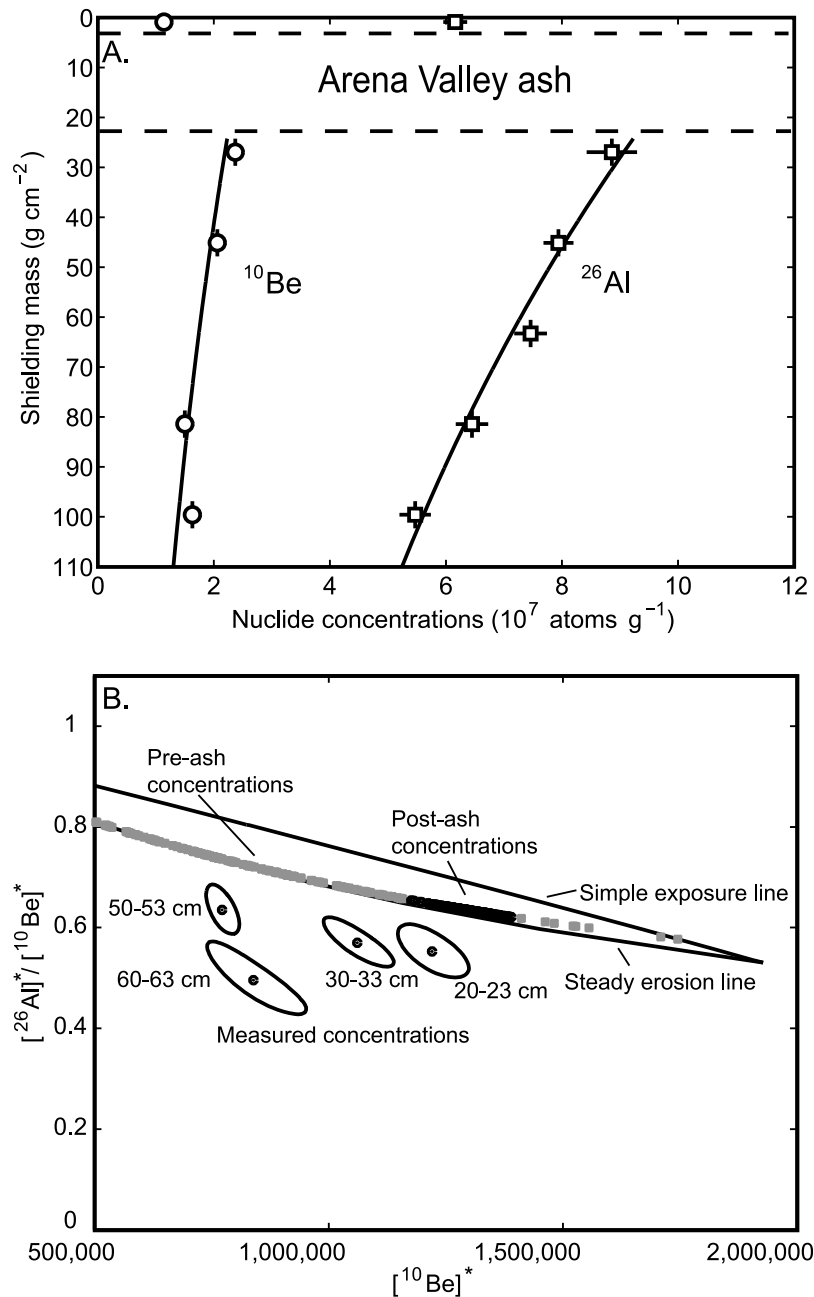

Figure 4

Table 2. Comparing the Best Fit Values of Each Exposure Model for Each Sample Site

Exposure Model	Unknowns	Arena Valley Ash 04-AV-Pit 4	Hart Ash 04-LWV-Pit 25
Equation (3)	Inherited ^{10}Be (at g^{-1})	9.4×10^5	9.2×10^5
Well-mixed	Inherited ^{26}Al (at g^{-1})	$\sim$0	$\sim$0
inherited nuclides	ε: Erosion after ash (g cm^{-2} yr^{-1})	3.3×10^{-5}	4.8×10^{-4}
	Reduced chi square value	1.7	3.5
Equation (4)	ε_1: Erosion before ash (g cm^{-2} yr^{-1})	1.0×10^{-4}	5.2×10^{-5}
Exponential profile for inherited nuclides	ε_2: Erosion after ash (g cm^{-2} yr^{-1})	3.5×10^{-5}	5.4×10^{-4}
Equation (5)	Reduced chi square value	1.3	3.7
Burial scenario	Inherited ^{10}Be (at g^{-1})	Not applicable	4.1×10^6
	ε_1: Erosion after ash (g cm^{-2} yr^{-1})		3.1×10^{-4}
	t_1: Time before burial (Ma)		0.4
	t_b: Burial time (Ma)		2.2
	ε_2: Erosion after burial (g cm^{-2} yr^{-1})		5.0×10^{-4}
	t_2: Exposure time since burial (Ma)		1.3
	Reduced chi square value		6.7

happened at this site in the past ~4 Ma. To further explore the possibility that the samples record information about the erosion rate before the ash was deposited, we begin by assuming that any ^{26}Al from before the ash would have decayed to essentially zero in the intervening 4.33 Ma, that the ^{26}Al concentrations in the samples today are the result of only the period of erosion after the ash was deposited. Then, we predict the ^{10}Be concentrations from the erosion rate indicated by the ^{26}Al. Any ^{10}Be in excess of this prediction would then be inherited from before the ash was emplaced.

[33] When we fit an erosion rate to only the ^{26}Al data, we get an erosion rate of 4.1×10^{-5} g cm^{-2} yr^{-1} with a reduced chi square fit of 0.71. The ^{10}Be concentrations predicted by this erosion rate fit within the error of the measured ^{10}Be concentrations, so we cannot conclude anything about the erosion rate before the ash was emplaced with this method. However, if the erosion rate before the ash was lower than it has been since the ash was deposited, then there should be higher ^{10}Be concentrations in the samples than what was measured, which suggests that the erosion rate before the ash had to have been higher than it has been for the past 4.33 Ma. Although the data do suggest that the erosion rate before the ash was deposited was higher than it was afterward, we can only conclusively say that these measurements indicate that steady erosion at a rate of 3.5×10^{-5} g cm^{-2} yr^{-1} has been occurring for the past ~4 Ma because the nuclide concentrations have come into equilibrium with production, decay, and loss due to erosion in this amount of time.
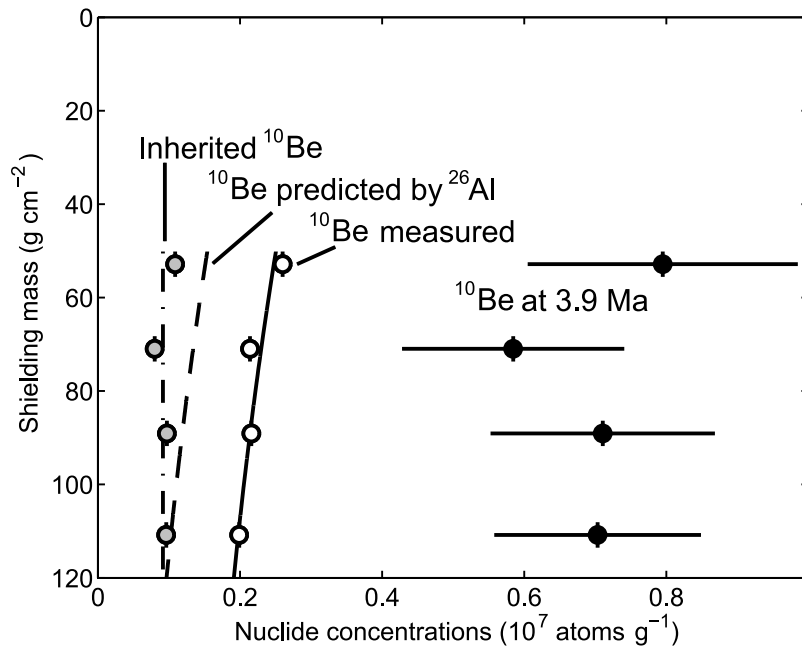
4.2. The Hart Ash

[34] From the geologic description of the Hart ash site and the observations of *Hall et al.* [1993], we expect that the nuclide concentrations from the colluvium below the Hart ash will reflect cryoturbation and erosion before the deposition of the ash and possibly either erosion, burial, or a combination of these processes after the ash was emplaced. The nuclide concentrations of the colluvium below the Hart ash yield simple exposure ages of only ~200–500 ka, which is much younger than the overlying 3.9 Ma Hart ash, which indicates that the nuclide concentrations are better interpreted as representing either the degradation rate of the regolith or burial at the site.

[35] The nuclide concentrations for the samples beneath the Hart ash fit equation (3) with a reduced chi square value of 3.5 and fit equation (4) with a reduced chi square value of 3.7, indicating that a constant, well-mixed profile for the inherited

Figure 4. (a) Measured ^{10}Be (circles) and ^{26}Al (squares) concentrations (atoms g$^{-1}_{quartz}$) at the Arena Valley ash site (04-AV-Pit 4). The small vertical and horizontal lines indicate the range of depth of the sediment sampled and the error in the nuclide measurement, respectively. In some cases, these values are smaller than the markers used to indicate each datum. The white box shows the approximate location of the Arena Valley ash in the soil column. The solid lines show the predicted nuclide concentrations for the best fit model results where the erosion rate before the ash was $1.0 \pm 0.40 \times 10^{-4}$ g cm^{-2} yr^{-1} and that after the emplacement of the ash the erosion rate was $3.5 \pm 0.41 \times 10^{-5}$ g cm^{-2} yr^{-1}. (b) A Klein-Nishiizumi two-isotope diagram, which plots the ^{26}Al/^{10}Be ratio against the ^{10}Be concentration. Nuclide concentrations for each sample have been divided by the production rate of the nuclides at each sample depth, which is indicated by the asterisk in the axes labels. For each sample that we have of the concentrations of both ^{10}Be and ^{26}Al, the measurements are shown as black circles with ellipses around them, representing the 68% confidence interval. The general interpretation of this diagram is that cosmogenic nuclide concentrations that reflect only surface exposure plot on the upper line, concentrations that reflect erosion plot on the lower line, and concentrations that reflect a more complicated exposure history, such as burial or inheritance, plot below these lines. A more detailed explanation of this diagram can be found in the work of *Lal* [1991]and *Balco et al.* [2005b]. The gray boxes and black circles show the results of separating the measured concentrations into pre- and post-ash components, respectively. Each dot represents the realization of a 200 point Monte Carlo simulation. We have plotted only a 200 point simulation instead of the 10,000 point simulation for the ease of presentation, but the results are similar. The pre-ash components have been adjusted to indicate the erosion rate that would have been active at 4.33 Ma just before the ash was deposited. In the subsequent 4.33 Ma, these nuclide concentrations would have decayed significantly. Both pre- and post-ash components plot directly on the steady erosion line, indicating that the measured nuclide concentrations can be explained by erosion alone and do not indicate that the sample site has been buried at any point in the past ~4 Ma.
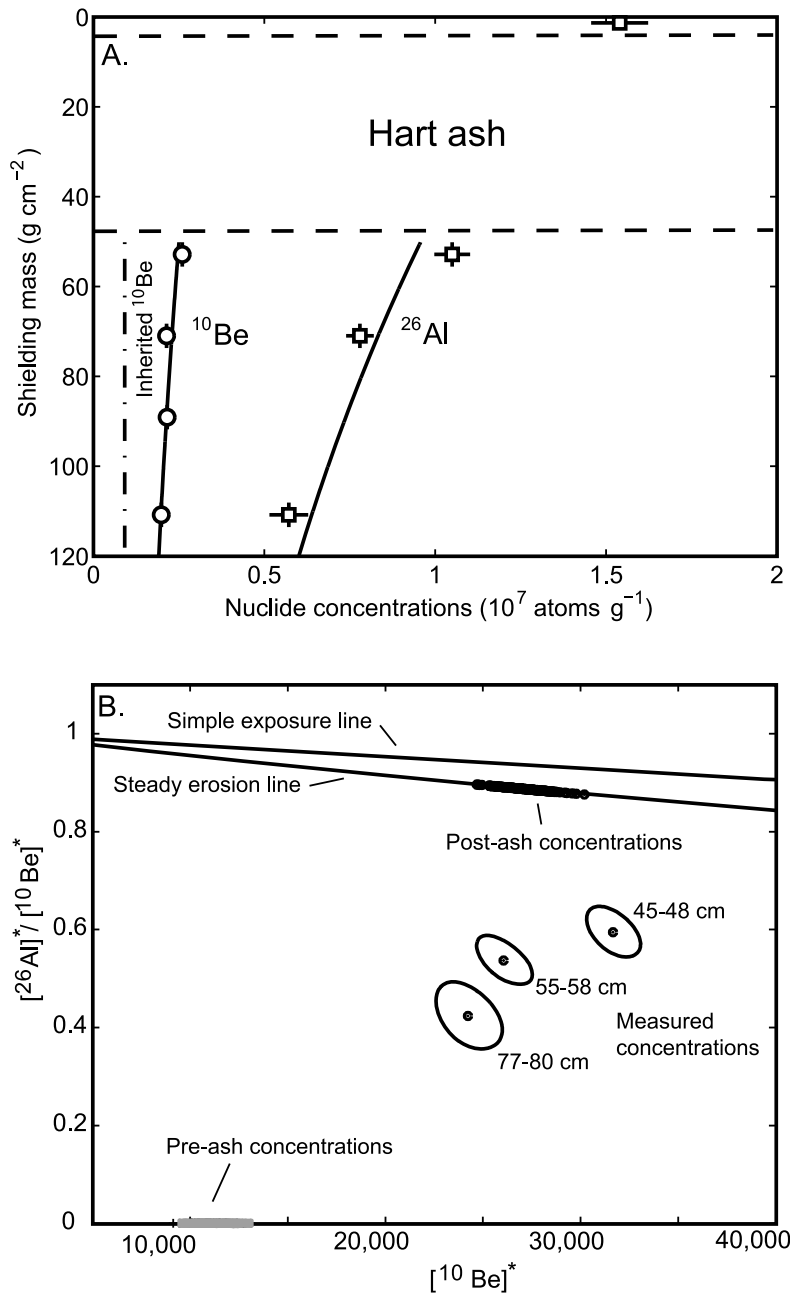
Figure 5. (a) Measured ^{10}Be (circles) and ^{26}Al (squares) concentrations (atoms g^{-1}_{quartz}) at the Hart ash site (04-LWV-Pit 25). The small vertical and horizontal lines indicate the range of depth of the sediment sampled and the error in the nuclide measurement, respectively. In some cases, these values are smaller than the markers used to indicate each datum. The white box shows the approximate location of the Hart ash. The dash-dotted vertical line shows the calculated inherited ^{10}Be from before the ash was deposited that remains in the soil today. The solid lines show the best fit model results of zero inherited ^{26}Al, $9.2 \pm 0.67 \times 10^5$ at g^{-1} inherited ^{10}Be remaining in the samples today, and an erosion rate of $4.8 \pm 0.21 \times 10^{-4}$ g cm^{-2} yr^{-1} for the past 3.9 Ma. Because an erosion rate this fast will cause nuclide concentrations to reach a steady state between production and decay in 1 Ma, all that we can conclusively say is that erosion at a rate of $4.8 \pm 0.21 \times 10^{-4}$ g cm^{-2} yr^{-1} has gone on for the past ~1 Ma. (b) A Klein-Nishiizumi two-isotope diagram for the Hart ash site and is plotted in the same format as Figure 4b. Although the measured nuclide concentrations plot below the steady erosion line, they can be separated into pre- and post-ash components that indicate that the site has been steadily eroding for the past ~1 Ma and has not been buried by ice during this period. The pre-ash components lie at the bottom of the plot because there is essentially zero ^{26}Al left in the samples from before the ash was deposited but do not indicate that the site was buried before the deposition of the ash. The pre-ash ^{10}Be component lie in a nearly vertical line, which is reflective of vertical mixing, likely due to cryoturbation that was active at the site before the ash was emplaced.

Figure 6. Analyzing the inherited [10]Be concentrations below the Hart ash. The measured concentrations of [10]Be are shown by the open circles. The solid line shows the best fit line through the [10]Be data and the vertical dash-dotted line shows the predicted well-mixed inherited [10]Be remaining in the sediment today (9.2×10^5 atoms g^{-1}) from the analysis shown in Figure 5. The dashed line shows the amount of [10]Be predicted by the best fit erosion rate for the [26]Al concentrations. The gray circles are the difference between the measured [10]Be concentration and the [10]Be concentration predicted by the [26]Al erosion rate, which in this analysis is assumed to be the inherited [10]Be left in these samples. These calculated inherited [10]Be concentrations nearly fall along the well-mixed inheritance line. The black circles show the value of the inherited [10]Be at 3.9 Ma when the Hart ash was deposited. That is, if we decay the [10]Be concentrations in the black circles for 3.9 Ma, we get the values of the gray circles. The nuclide concentrations at the time the ash was deposited predicted by this exercise are higher than the measured concentrations in the samples today, which may indicate that erosion at this site before the ash was emplaced was lower than it is today.

nuclides fits the measurements better than an exponential profile (Table 2; contour plots of the chi square fits for these exposure models are shown in Appendix B). This indicates that the inherited nuclide component reflects vertical mixing of the sediment due to cryoturbation before the Hart ash was deposited. The results from equation (3) show that there is essentially zero inherited [26]Al, $9.2 \pm 0.67 \times 10^5$ at g^{-1} inherited [10]Be remaining in the samples today, and an erosion rate of $4.8 \pm 0.21 \times 10^{-4}$ g cm^{-2} yr^{-1} for the time period that the measurements reflect (Figure 5a). On the basis of the effective half-life of the nuclides under this erosion rate, these concentrations record what has happened at this site in the past ~1 Ma. Figure 5a shows the measured nuclide concentrations and the predicted nuclide concentrations for erosion rate of $4.8 \pm 0.21 \times 10^{-4}$ g cm^{-2} yr^{-1}. Because the measured nuclide concentrations fit equation (3) well, no vertical mixing of the soil has occurred in the last ~1 Ma, but vertical mixing is indicated by the inherited nuclide component before the ash was deposited at 3.9 Ma.

[36] Because *Hall et al.* [1993] suggest that the sample site may have been overridden by a glacier, we must test for the possibility of burial and shielding of these samples from cosmic rays. Figure 5b shows the nuclide concentrations plotted on a Klein-Nishiizumi two-isotope diagram and the measured nuclide concentrations plot below the steady erosion line, which suggests that the samples may have been

shielded. By separating the nuclide concentrations in the pre- (gray boxes) and post-ash (black circles) components following equation (3), we see that the post-ash components plot on the steady erosion line, indicating that the samples have not been buried in the time period that they record, which is only the past ~1 Ma. The pre-ash component plots well below the steady erosion line, but this is because the pre-ash [26]Al concentrations are essentially zero.

[37] We can also test for the possibility of burial by ice by fitting equation (5) to the measured nuclide concentrations. In this scenario, we have five unknowns (inherited [10]Be, two erosion rates, and two time periods) and only seven data points, so the fit may not be as well constrained as it is in the other exposure models. The results of the best fit scenario are for a well-mixed inherited [10]Be concentration of 4.1×10^6 at g^{-1} at the time the ash was deposited, an erosion rate of 3.1×10^{-4} g cm^{-2} yr^{-1} for the 0.4 Ma after the ash was deposited, a burial period of 2.2 Ma, followed by an erosion rate of 5.0×10^{-4} g cm^{-2} yr^{-1} for 1.3 Ma after the burial until today. These results fit the data with a reduced chi square value of 6.7. Because the chi square fit is not as good for this exposure model, burial is not necessary to explain the data, and ultimately, this exposure model yields the same result as the erosion and inheritance exposure model in equation (3), that there has been erosion of ~5×10^{-4} g cm^{-2} yr^{-1} for the past ~1 Ma (Table 2). [10]Be and [26]Al concentrations will come into
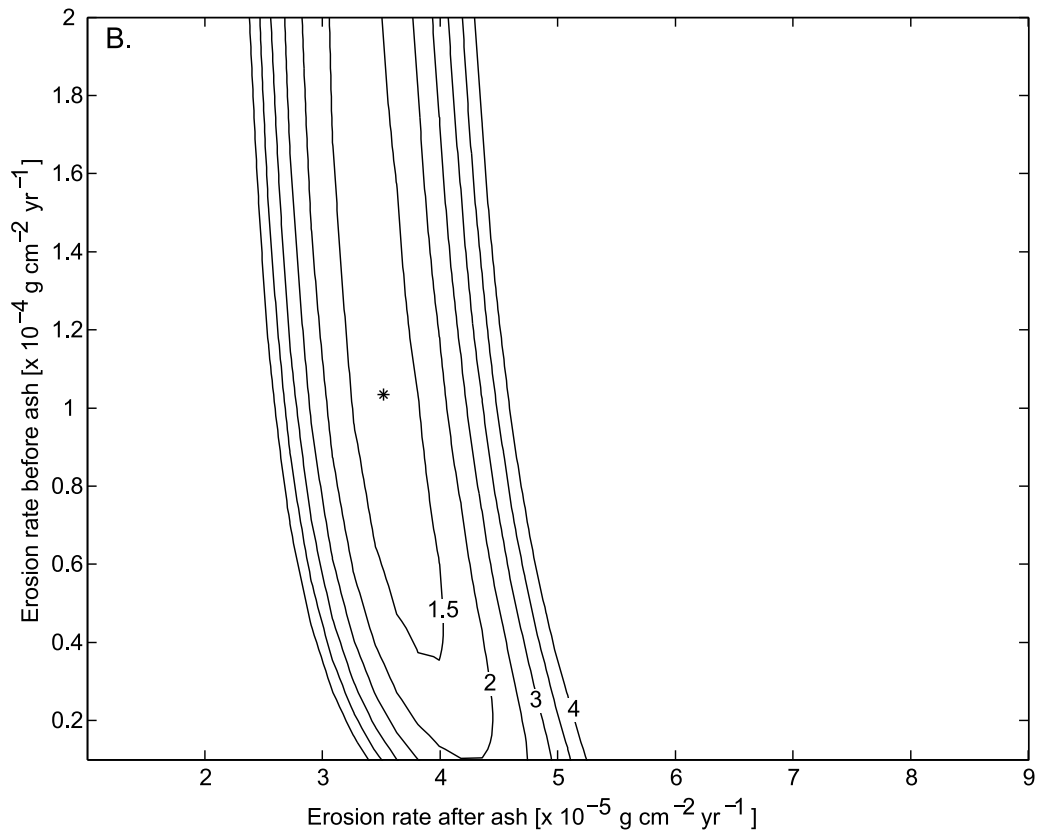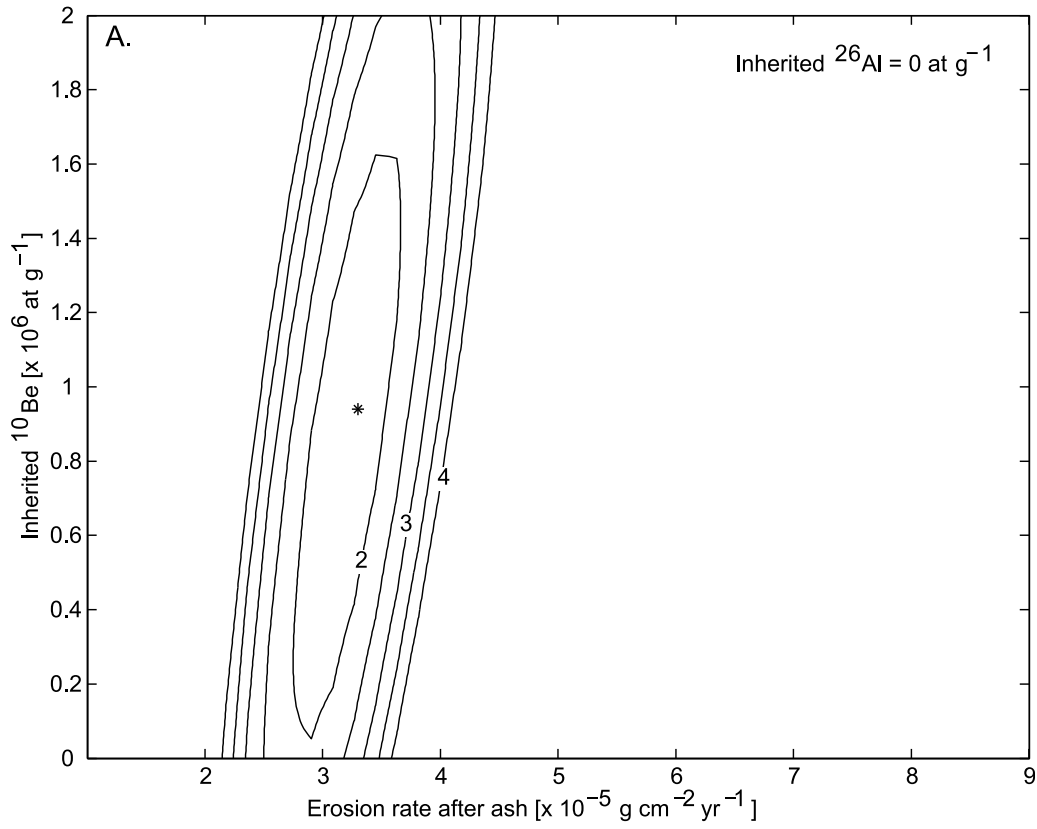
Figure A1

equilibrium with an erosion rate of ~5×10^{-4} g cm^{-2} yr^{-1} in ~1 Ma, effectively removing any information that we have about burial, so we can only conclusively say that erosion at this rate has gone on for the last ~1 Ma.

[38] Given that the Hart ash is 3.9 Ma, it makes sense not to have any inherited ^{26}Al left in these samples because only ~3% of any inherited ^{26}Al should theoretically remain in the samples, and this is smaller than the analytical uncertainties in the ^{26}Al measurements. Following the same reasoning we described for the Arena Valley ash, we can further examine the inherited nuclide concentrations by assuming that the measured ^{26}Al concentrations are the result of erosion for the past 3.9 Ma and predicting the ^{10}Be concentrations from the erosion rate indicated by the ^{26}Al measurements. The expected erosion rate from the ^{26}Al concentrations is 5.0×10^{-4} g cm^{-2} yr^{-1}, which is slightly higher than the previous fit, but within the error of the results. The ^{10}Be concentrations predicted by this erosion rate are less than the measured ^{10}Be concentrations (Figure 6), which is consistent with the idea that there is some ^{10}Be remaining in the samples that is attributable to exposure before the deposition of the ash. If we subtract the predicted ^{10}Be concentrations from the measured ^{10}Be concentrations and assume that the difference is the inherited ^{10}Be, then the resulting inherited ^{10}Be profile is more or less vertical, which is consistent with the idea that the site experienced cryoturbation before the ash was deposited and should be well mixed. This reaffirms the notion that the site was experiencing cryoturbation before the ash was emplaced, resulting in a well-mixed inherited nuclide profile.

4.3. Samples Above the Ash

[39] The final observation is that at both sites the nuclide concentrations for the samples above the ash are different than what is predicted by the erosion rate indicated by the samples below the ash. Stratigraphically, these samples are different from the ash layers that they overlie, so their exposure history is not necessarily related to either the underlying ash or colluvium. At both sample sites, the samples above the ash came from the uppermost layer of ash that was mixed with quartz sands. Our interpretation of the surface samples is that they represent material that is actively moving at the surface today, as observed by *Putkonen et al.* [2007]. This material could be moving downslope or it could be wind blown, but regardless of the method of transportation, this upper sample contains cosmogenic nuclide concentrations that are unrelated to those that are below the ash.

[40] At the Arena Valley ash site, the simple exposure age for the sample from 0 to 1 cm depth is ~600 ka, which corresponds to an erosion rate of 1.8×10^{-4} g cm^{-2} yr^{-1} for the past ~2.6 Ma, which is much higher than the erosion rate indicated by the samples below the ash. Because the erosion rate of the surface sample is so high, we cannot create an exposure model where the samples below the ash accumulate enough nuclides in the first ~1.73 Ma of exposure since the ash was deposited to reach their measured concentrations. The result is that the erosion rate of the surface sample cannot have been the erosion rate of the entire sediment package for the past ~2.6 Ma and the nuclide concentrations of the sample above the ash are unrelated to those from the colluvium below the ash.

[41] For the sample above the Hart ash, we only have a ^{26}Al measurement, and it is a higher concentration than expected, given the steady erosion rate determined from the colluvium below the ash. The ^{26}Al concentration of this sample gives a simple exposure age of 280 ka and an erosion rate of 4.2×10^{-4} g cm^{-2} yr^{-1} for the past ~1.2 Ma. This erosion rate is ~20% lower than the best fit erosion rate for the sample below the ash. If this is the erosion rate that has gone on for the past ~1.2 Ma (the time period that this sample records), then the concentration of ^{26}Al in the samples below the ash would have to be much higher than measured. Again, our interpretation of the surface sample is that it represents material that is actively being transported and is unrelated stratigraphically to the material below it.

5. Discussion

5.1. Erosion Rates of Regolith in the MDV

[42] At both of the sample sites, we are able to use the cosmogenic nuclide concentrations to address questions about the nature of the exposure that each of these sites has experienced. This includes the erosion rates both before and after the ashes were deposited, the potential for vertical mixing and cryoturbation at each site, and the possibility of burial by cold-based ice and shielding from cosmic rays. At both of the ash sites, the concentrations of ^{10}Be and ^{26}Al both above and below the ash deposits are lower than expected given the ages of the ashes, burial of these sites after the ashes were deposited is not indicated by the exposure models or the ^{26}Al/^{10}Be ratio in the time period that the measurements record, and the nuclide concentrations are best interpreted as degradation rates.

Figure A1. (a) Contour plots of the reduced chi square value for the combination of inherited ^{10}Be and erosion rate after the ash was deposited in the exposure model described by equation (3) for the Arena Valley ash site (04-AV-Pit 4). Contours are plotted at an interval of 0.5. This plot has the inherited ^{26}Al value set to 0 at g^{-1}, which is the amount that best fits the data and allows for the lowest reduced chi square value, which is 1.7 when the unknown values are 9.4×10^{5} atoms g^{-1} for the inherited ^{10}Be and an erosion rate of 3.2×10^{-5} g cm^{-2} yr^{-1} after the ash was deposited (black star). From this plot, it is clear that there is a tight constraint on the value for the erosion rate after the ash was emplaced. (b) Contour plots of the reduced chi square value for the combination of erosion rates before and after the ash was deposited in the exposure model described by equation (4) for the Arena Valley ash site (04-AV-Pit 4). Contours are plotted at an interval of 0.5. The data indicate the lowest reduced chi square value of 1.3 is met when the erosion rate before the ash was deposited is 1.0×10^{-4} g cm^{-2} yr^{-1} and the erosion rate is 3.5×10^{-5} g cm^{-2} yr^{-1} after the ash was deposited (black star). From this plot, it is clear that if the erosion rate before the ash was deposited is lower than it is after the ash (~4×10^{-5} g cm^{-2} yr^{-1}), then the fit worsens. Though this is not a conclusive result, this does support the idea that erosion rate before the ash was deposited was higher than it has been for the past ~4 Ma. It is also apparent from this plot that there is a much tighter constraint on the value for the erosion rate after the ash was emplaced than there is for the erosion rate before the ash.
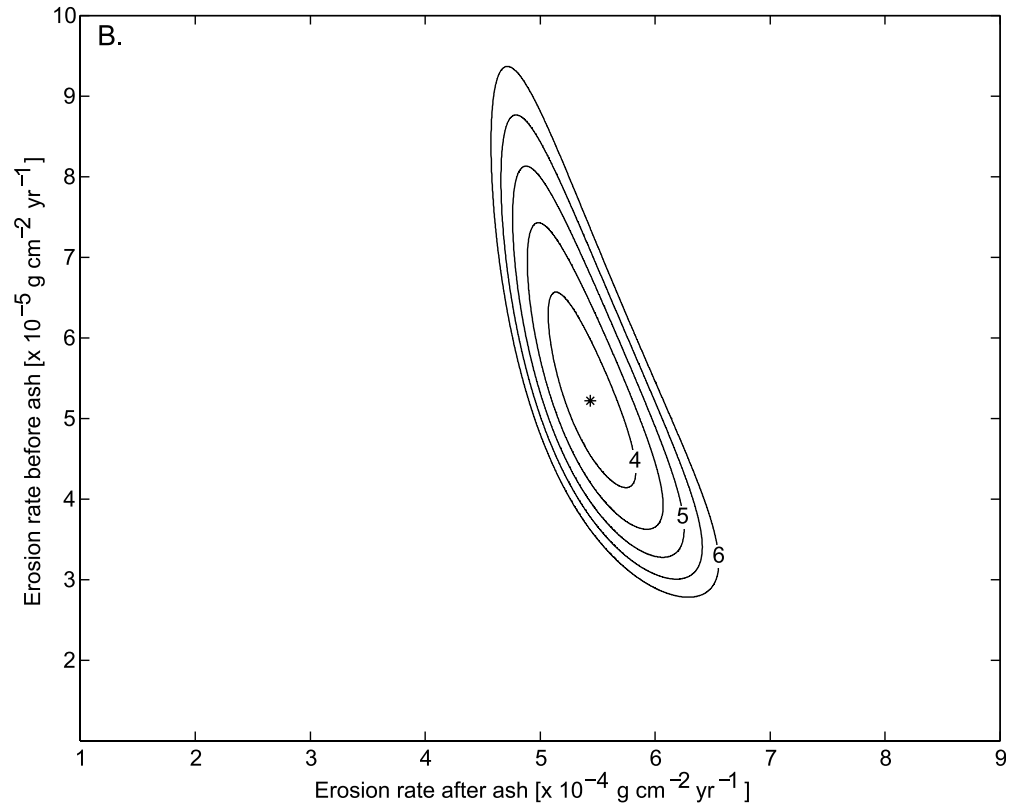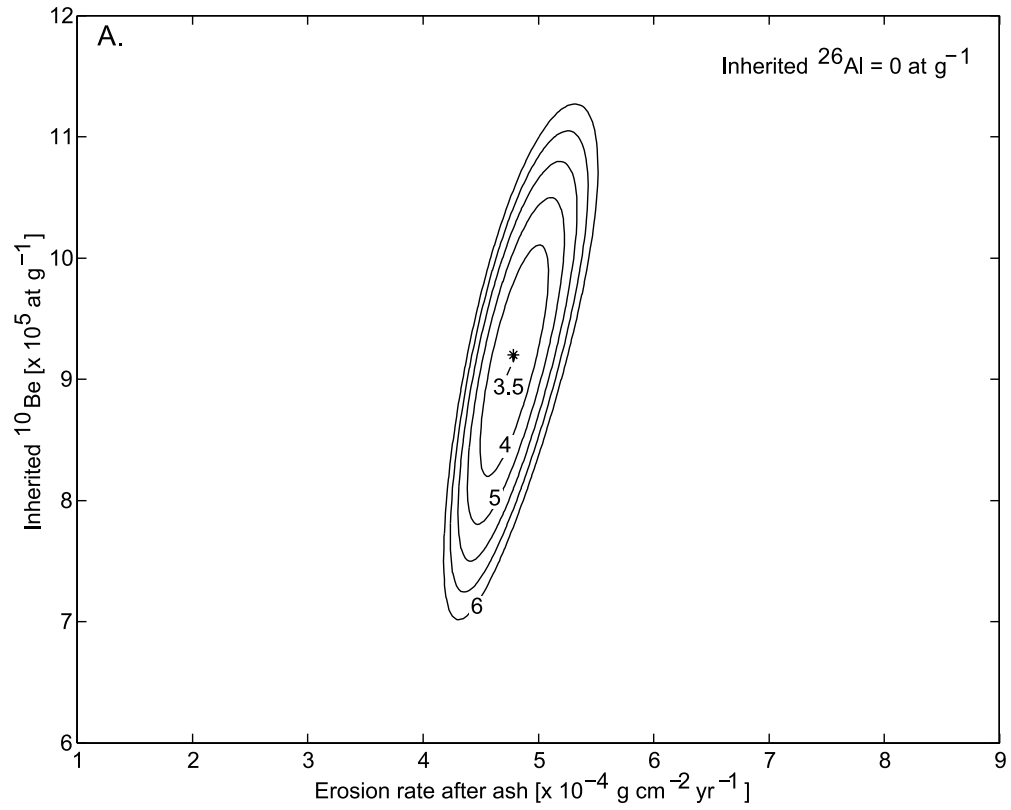
Figure B1

[43] The erosion rate results are given in units of g cm^{-2} yr^{-1}, which reflects the amount of shielding that has been removed from the surface and is independent of the density of the material removed. We report the erosion rates this way because we do not know if the ash was originally thicker, if it was covered by more regolith, or by some combination of these materials. If we assume that the density of the material removed was at least that of the ash and no greater than the regolith, we can put a range on the amount of material removed at each site. Using an average density of 1.01 g cm^{-3} for the ash and 1.81 g cm^{-3} for the regolith (Table 1), we calculate an erosion rate of 0.19–0.35 m Ma^{-1} at the Arena Valley ash site and 2.6–4.7 m Ma^{-1} at the Hart ash site. Because we only know that erosion has been occurring at the Arena Valley ash site for ~4 Ma and at the Hart ash site for ~1 Ma, the net removal of material over these time periods is 0.76–1.4 m at the Arena Valley ash site and 2.6–4.7 m at the Hart ash site. *Putkonen et al.* [2008] found that a landslide deposit in Arena Valley was eroding at a rate of 2.1 m Ma^{-1} for at least the past ~2 Ma, which is an order of magnitude higher than the erosion rate at the Arena Valley ash site determined in this study. At the Hart ash site, the results are consistent with those found by *Schiller et al.* [2009], who used atmospherically produced ^{10}Be to determine erosion rates of only 0.5 m Ma^{-1} before the Hart ash was deposited and 2.8 m Ma^{-1} after the ash was deposited.

[44] These results also suggest that erosion at these sites is stable over the time scales that the measurements record. Erosion in the MDV is not likely to be completely steady through time and is probably punctuated by episodes of relatively rapid erosion due to slope failures or high-wind events. The erosion rates reported in this study are slow and are comparable to the lowest rock erosion rates reported, which also come from arid regions [*Cockburn et al.*, 1999; *Summerfield et al.*, 1999; *Belton et al.*, 2004; *Dunai et al.*, 2005]. Under these slow erosion rates, the effective half-lives of the nuclides are quite large, which means that the measured nuclide concentrations integrate erosion over a very long period of time, on the order of 10^5–10^6 years. This means that the nuclide concentrations are very well buffered against changes in the erosion rate that occur on short time scales, and that on time scales on the order of 10^5–10^6 years, erosion at these sites is steady.

[45] There is an order of magnitude difference in the erosion rates between the Arena Valley and Hart ash sites, and this is likely related to either the different microclimate zones that these sites are located in or the different material that caps each ash deposit. Elevation, distance from the coast, mean annual temperature, relative humidity, exposure to and protection from high-velocity winds all affect erosion rates in the MDV [*Marchant and Head*, 2007]. Distinguishing the relative effects of these processes at each site is beyond the scope of this paper, but these results are consistent with the notion that microclimate variations in the MDV will result in different erosion rates [e.g., *Marchant and Denton*, 1996; *Marchant and Head*, 2007]. The erosion rates determined in this study for the stable upland zone (where the Arena Valley ash lies) are lower than those in the inland mixed zone (where the Hart ash lies). Additionally, these results suggest that the higher erosion rate at the Hart ash site could be related to the fact that the site is capped by a gravel lag consisting of granitoid pebbles that weathers more quickly and provides less armor than the dolerite-rich desert pavement that caps the Arena Valley ash. This notion is consistent with the idea proposed by *Lancaster* [2002] that erosion rates in the MDV are more influenced by the availability of material than by just wind speed.

[46] The observation that millions of years old surface deposits in the MDV maintain their meter-scale morphology despite the fact that they are eroding is likely related to the lack of creep that has been documented at these sites. Creep is a common process of soil erosion in a variety of environments [*Oehm and Hallet*, 2005] and in temperate regions has been shown to move soil downslope at depth-averaged rates on the order of ~10 m ka^{-1} [*Heimsath et al.*, 2002]. As shown by numerous solifluction and gelifluction lobes found in the MDV, creep is an active geomorphic process in some parts of the MDV, but creep has not been active at either the Arena Valley ash site for the past ~4 Ma or the Hart ash site for the past ~1 Ma. Erosion at these sites appears to operate by simply lowering the surface over time. The cosmogenic nuclide concentrations of the surface samples at each site reaffirm the notion that there is a thin layer of actively transported material, but that below a few centimeters, the regolith is quite stable. This may explain how some surface deposits in the MDV maintain their meter-scale morphology for millions of years while uniformly eroding a few meters over that time period. By simply lowering over time without creep, there is not likely to be much downslope movement of material, and the basic shape of landforms can be preserved over time.

5.2. Implications for Glacial History

[47] On the basis of the observations of *Hall et al.* [1993], it is possible that the Hart ash has been covered by ice at some

Figure B1. (a) Contour plots of the reduced chi square value for the combination of inherited ^{10}Be and erosion rate after the ash was deposited in the exposure model described by equation (3) for the Hart ash site (04-LWV-Pit 25). Contours are plotted at an interval of 0.5. The 3.5 contour is smaller than the black star on the plot. This plot has the inherited ^{26}Al value set to 0 at g^{-1}, which is the amount that best fits the data and allows for the lowest reduced chi square value, which is 3.5 when the unknown values are 9.2×10^5 atoms g^{-1} for the inherited ^{10}Be and an erosion rate of 4.8×10^{-4} g cm^{-2} yr^{-1} after the ash was deposited (black star). From this plot, it is clear that there is a tight constraint on the value for the erosion rate after the ash was emplaced. Because this exposure model captures more of the data than equation (4) or (5), we conclude that the inherited nuclides remaining in the colluvium below the Hart ash represent vertical mixing, probably related to cryoturbation, more than they represent any erosion that occurred at the site before the ash was deposited. (b) Contour plots of the reduced chi square value for the combination of erosion rates before and after the ash was deposited in the exposure model described by equation (4) for the Hart ash site (04-LWV-Pit 25). Contours are plotted at an interval of 0.5. The data indicate the lowest reduced chi square value of 3.7 is met when the erosion rate before the ash was deposited is 5.2×10^{-5} g cm^{-2} yr^{-1} and the erosion rate is 5.4×10^{-4} g cm^{-2} yr^{-1} after the ash was deposited (black star).

point after it was deposited. *Hall and Denton* [2005] suggest that sea ice may have reached an elevation of 750 m in Eastern Wright Valley in the late Pliocene The results of this study show that Hart ash site has not been buried by ice or water in the past ~1 Ma. Although we can create a well-fitting exposure model that includes burial at this site for 2.2 Ma followed by erosion for 1.3 Ma, the dominant signature in the nuclide concentrations is erosion for the past ~1 Ma. On the basis of the surrounding geomorphology, the Hart ash site does not appear to have been covered by ice or water since it was deposited. *Hall et al.* [1993] extensively mapped the glacial deposits from the local alpine glaciers, and the Hart ash site lies outside of the limit that these glaciers reached. The Hart ash site is also above the 300 m elevation limit of fjord deposits found in Wright Valley [*Hall et al.*, 1993; *Prentice and Krusic*, 2005]. *Prentice and Krusic* [2005] limit the last expansion of ice in Lower Wright Valley to between 5.5 ± 0.4 and 3.7 ± 0.1 Ma. Thus, though the scenario that the site has been covered by cold-based ice is mathematically possible, it is not necessary and all that we can conclusively say is that the Hart ash site has been eroding at a rate of $4.8 \pm 0.21 \times 10^{-4}$ g cm^{-2} yr^{-1} for the past ~1 Ma and that it was not buried by ice during this period.

6. Conclusions

[48] We examined how regolith degrades in the cold, polar desert climate of the McMurdo Dry Valleys, Antarctic for the past ~1–4 Ma by measuring the concentration of ^{10}Be and ^{26}Al above and below two ash deposits. At both of the ash sites, the concentration of ^{10}Be and ^{26}Al both above and below the ash deposits are lower than expected given the ages of the ashes. Burial by weakly erosive, cold-based ice cannot explain these low nuclide concentrations at the Arena Valley ash site, and at the Hart ash site, burial is possible but is indistinguishable from erosion for the past ~1 Ma. The measured nuclide concentrations reflect erosion at these sites at a rate of $3.5 \pm 0.41 \times 10^{-5}$ g cm^{-2} yr^{-1} (0.19 m Ma^{-1} of regolith or 0.35 m Ma^{-1} of ash) for the past ~4 Ma at the Arena Valley ash site and an erosion rate of $4.8 \pm 0.21 \times 10^{-4}$ g cm^{-2} yr^{-1} (2.6 of regolith or 4.7 m Ma^{-1} of ash) for the past ~1 Ma at the Hart ash site. While these rates are slow, they are measurable, and at both of these sites, there is no indication of soil creep or vertical mixing of the sediment in the time period that the measurements record. The cosmogenic nuclide concentrations in the samples above the ash do not have the same exposure history as those below the ash, supporting the idea that regolith degradation at these sites is limited to the upper few centimeters of the regolith. Erosion without creep would result in the steady lowering of the surface, which may help to preserve the meter-scale morphology of millions of years old surface deposits in the MDV. These results reaffirm the notion that the MDV are a geomorphologically unique environment where erosion occurs at very slow rates and, in some cases, without soil creep.

Appendix A

[49] Figure A1 shows contour plots of the reduced chi square value for the combination of inherited ^{10}Be and erosion rate after the ash was deposited in the exposure model described by equation (3) for the Arena Valley ash site (04-

AV-Pit 4) (Figure A1a), and contour plots of the reduced chi square value for the combination of erosion rates before and after the ash was deposited in the exposure model described by equation (4) for the Arena Valley ash site (04-AV-Pit 4) (Figure A1b).

Appendix B

[50] Figure B1 shows contour plots of the reduced chi square value for the combination of inherited ^{10}Be and erosion rate after the ash was deposited in the exposure model described by equation (3) for the Hart ash site (04-LWV-Pit 25) (Figure B1a), and contour plots of the reduced chi square value for the combination of erosion rates before and after the ash was deposited in the exposure model described by equation (4) for the Hart ash site (04-LWV-Pit 25) (Figure B1b).

References

Balco, G., and D. L. Shuster (2009), Production rate of cosmogenic ^{21}Ne in quartz estimated from ^{10}Be, ^{26}Al, and ^{21}Ne concentrations in slowly eroding Antarctic bedrock surfaces, *Earth Planet Sci. Lett.*, *281*(1–2), 48–58, doi:10.1016/j.epsl.2009.02.006.

Balco, G., J. Stone, and C. Jennings (2005a), Dating Plio-Pleistocene glacial sediments using the cosmic-ray-produced radionuclides ^{10}Be and ^{26}Al, *Am. J. Sci.*, *305*(1), 1–41, doi:10.2475/ajs.305.1.1.

Balco, G., J. Stone, and J. Mason (2005b), Numerical ages for Plio-Pleistocene glacial sediment sequences by ^{26}Al/^{10}Be dating of quartz in buried paleosols, *Earth Planet Sci. Lett.*, *232*(1–2), 179–191.

Belton, D. X., R. W. Brown, B. P. Kohn, D. Fink, and K. A. Farley (2004), Quantitative resolution of the debate over antiquity of the central Australian landscape: implications for the tectonic and geomorphic stability of cratonic interiors, *Earth Planet Sci. Lett.*, *219*(1–2), 21–34.

Bockheim, J. G. (2002), Landform and Soil Development in the McMurdo Dry Valleys, Antarctica: A Regional Synthesis, *Arct. Antarct. Alp. Res.*, *34*(3), 308–317.

Campbell, I. B., and G. G. C. Claridge (1969), A classification of frigic soils-the zonal soils of the Antarctic continent, *Soil Sci.*, *107*, 75–85.

Campbell, I. B., and G. G. C. Claridge (1987), *Antarctica: Soils, Weathering Processes, and Environment*, Elsevier, New York.

Campbell, I. B., and G. G. C. Claridge (2006), Permafrost properties, patterns and processes in the Transantarctic Mountains region, *Permafrost Periglac.*, *17*, 215–232.

Chinn, T. J. (1990), *The Dry Valleys in Antarctica: The Ross Sea Region*, pp. 137–153, Dept. of Scientific and Industrial Research, Wellington, NZ.

Cockburn, H. A. P., M. A. Seidl, and M. A. Summerfield (1999), Quantifying denudation rates on inselbergs in the central Namib Desert using in situ-produced cosmogenic ^{10}Be and ^{26}Al, *Geology*, *27*(5), 399–402.

Denton, G., M. Prentice, D. Kellogg, and T. Kellogg (1984), Late Tertiary history of the Antarctic ice sheet; evidence from the dry valleys, *Geology*, *12*(5), 263–267.

Denton, G., D. Sugden, D. Marchant, B. Hall, and T. Wilch (1993), East Antarctic ice sheet sensitivity to Pliocene climatic change from a Dry Valleys perspective, *Geogr. Ann. A.*, *75*(4), 155–204.

Doran, P., C. McKay, G. Clow, G. Dana, A. Fountain, T. Nylen, and W. Lyons (2002), Valley floor climate observations from the McMurdo Dry Valleys, Antarctica, 1986–2000, *J. Geophys. Res.*, *107*(D24), 4772, doi:10.1029/2001JD002045.

Dunai, T. J., G. A. G. Lopez, and J. Juez-Larre (2005), Oligocene-Miocene age of aridity in the Atacama Desert revealed by exposure dating of erosion-sensitive landforms, *Geology*, *33*(4), 321–324.

Fernandes, N., and W. Dietrich (1997), Hillslope evolution by diffusive processes: The timescale for equilibrium adjustments, *Water Resour. Res.*, *33*(6), 1307–1318.

Fountain, A., et al. (1999), Physical controls on the Taylor Valley Ecosystem, Antarctica, *BioScience*, *49*(12), 961–971.

Gillespie, A. R., and P. R. Bierman (1995), Precision of terrestrial exposure ages and erosion rates estimated from analysis of cosmogenic isotopes produced in situ, *J. Geophys. Res.*, *100*(B12), 24,637–24,649.

Gosse, J., and F. Phillips (2001), Terrestrial in situ cosmogenic nuclides: Theory and application, *Quat. Sci. Rev.*, *20*(14), 1475–1560.

Hall, B. L., and G. H. Denton (2005), Surficial geology and geomorphology of eastern and central Wright Valley, Antarctica, *Geomorphology*, *64*(1–2), 25–65, doi:10.1016/j.geomorph.2004.05.002.

Hall, B., G. Denton, D. Lux, and J. Bockheim (1993), Late Tertiary Antarctic Paleoclimate and ice-sheet dynamics inferred from surficial deposits in Wright Valley, *Geogr. Ann. Ser. A*, *75*(4), 239–267.

Hanks, T. C. (2000), The age of scarplike landforms from diffusion-equation analysis, in *Quaternary Geochronology: Methods and Applications*, edited by J. S. Noller, J. M. Sowers, and W. R. Lettis, AGU, 582.

Hanks, T., R. Bucknam, K. Lajoie, and R. Wallace (1984), Modification of wave-cut and faulting-controlled landforms, *J. Geophys. Res.*, *89*(B7), 5771–5790.

Heimsath, A., J. Chappell, N. Spooner, and D. Questiaux (2002), Creeping soil, *Geology*, *30*(2), 111–114, doi:10.1130/0091-7613(2002)030<0111: CS>2.0.CO;2.

Lal, D. (1991), Cosmic ray labeling of erosion surfaces – in situ nuclide production rates and erosion models, *Earth Planet Sci. Lett.*, *104*, 424–439.

Lancaster, N. (2002), Flux of Eolian sediment in the McMurdo Dry Valleys, Antarctica: A preliminary assessment, *Arct. Antarct. Alp. Res.*, *34*(3), 318–323.

Lewis, A., D. Marchant, A. Ashworth, S. Hemming, and M. Machlus (2007), Major middle Miocene global climate change: Evidence from East Antarctica and the Transantarctic Mountains, *Geol. Soc. Am. Bull.*, *119*(11–12), 1449–1461, doi:10.1130/0016-7606(2007)119[1449: MMMGCC]2.0.CO;2.

MacClune, K., A. Fountain, J. Kargel, and D. MacAyeal (2003), Glaciers of the McMurdo dry valleys: Terrestrial analog for Martian polar sublimation, *J. Geophys. Res.*, *108*(E4), 5031, doi:10.1029/2002JE001878.

Marchant, D., and G. Denton (1996), Miocene and Pliocene paleoclimate of the Dry Valleys region, Southern Victoria land: A geomorphological approach, *Mar. Micropaleontol.*, *27*(1–4), 253–271.

Marchant, D., and J. Head III (2007), Antarctic dry valleys: Microclimate zonation, variable geomorphic processes, and implications for assessing climate change on Mars, *Icarus*, *192*(1), 187–222, doi:10.1016/j.icarus. 2007.06.018.

Marchant, D., G. Denton, and C. Swisher (1993a), Miocene-Pliocene-Pleistocene Glacial History of Arena Valley, Quartermain Mountains, Antarctica, *Geogr. Ann. A*, *75*(4), 269–302.

Marchant, D., G. Denton, D. Sugden, and C. Swisher (1993b), Miocene glacial stratigraphy and landscape evolution of the Western Asgard Range, Antarctica, *Geogr. Ann. A.*, *75*(4), 303–330.

Marchant, D., C. Swisher, D. Lux, D. West, and G. Denton (1993c), Pliocene Paleoclimate and East Antarctic ice-sheet history from surficial ash deposits, *Science*, *260*(5108), 667–670, doi:10.1126/science.260. 5108.667.

Marchant, D., G. Denton, C. Swisher, and N. Potter (1996), Late Cenozoic Antarctic paleoclimate reconstructed from volcanic ashes in the dry valleys region of southern Victoria Land, *Geol. Soc. Am. Bull.*, *108*(2), 181–194.

Naish, T., R. Powell, R. Levy, G. Wilson, R. Scherer, F. Talarico, L. Krissek, F. Niessen, M. Pompilio, and T. Wilson (2009), Obliquity-paced Pliocene West Antarctic ice sheet oscillations, *Nature*, *458*(7236), 322–328.

Nash, D. B. (1980), Forms of bluffs degraded for different lengths of time in Emmet County, Michigan, USA, *Earth Surf. Processes Landforms*, *5*, 331–345.

Nishiizumi, K. (2004), Preparation of 26Al AMS standards, in *Nuclear Instruments and Methods in Physics Research Section B: Beam Interactions With Materials and Atoms*, *223–224*, 388–392, doi:10.1016/j. nimb.2004.04.075.

Nishiizumi, K., M. Imamura, M. Caffee, J. Southon, R. Finkel, and J. McAninch (2007), Absolute calibration of 10Be AMS standards, in *Nuclear Instruments and Methods in Physics Research Section B: Beam Interactions With Materials and Atoms*, *258*(2), 403–413, doi:10.1016/j. nimb.2007.01.297.

Oehm, B., and B. Hallet (2005), Rates of soil creep, worldwide: Weak climatic controls and potential feedback, *Z. Geomorphol.*, *49*, 353–372.

Prentice, M., and A. Krusic (2005), Early Pliocene alpine glaciation in Antarctica: Terrestrial versus tidewater glaciers in Wright Valley, *Geogr. Ann. A.*, *87*(1), 87–109.

Putkonen, J., and M. O'Neal (2006), Degradation of unconsolidated Quaternary landforms in the western North America, *Geomorphology*, *75*(3–4), 408–419.

Putkonen, J., R. Sletten, and B. Hallet (2003), Atmosphere/ice energy exchange through thin debris cover in Beacon Valley, *Antarctica*, 913–915.

Putkonen, J., M. Rosales, N. Turpen, D. Morgan, G. Balco, and M. Donaldson (2007), Regolith transport in the Dry Valleys of Antarctica, in *Antarctica: A Keystone in a Changing World—Online Proceedings of the 10th ISAES X*, edited by A. K. Cooper and C. R. Raymond et al., *USGS Open-File Report, U.S. Geological Survey Open-File Report 2007-1047*.

Putkonen, J., G. Balco, and D. Morgan (2008), Slow regolith degradation without creep determined by cosmogenic nuclide measurements in Arena Valley, Antarctica, *Quat. Res.*, *69*(2), 242–249, doi:10.1016/j. yqres.2007.12.004.

Schäfer, J., S. Ivy-Ochs, R. Wieler, I. Leya, H. Baur, G. Denton, and C. Schluchter (1999), Cosmogenic noble gas studies in the oldest landscape on Earth: Surface exposure ages of the Dry Valleys, Antarctica, *Earth Planet Sci. Lett.*, *167*(3–4), 215–226.

Schiller, M., W. Dickinson, R. G. Ditchburn, I. J. Graham, and A. Zondervan (2009), Atmospheric ^{10}Be in an Antarctic soil: Implications for climate change, *J. Geophys. Res.*, *114*, F01033, doi:10.1029/2008JF001052.

Stone, J. (2000), Air pressure and cosmogenic isotope production, *J. Geophys. Res.*, *105*(B10), 23,753–23,760.

Stone, J. (2004), Extraction of Al and Be from quartz for isotopic analysis, [online]. (Available from: http://depts.washington.edu/cosmolab/chem. html)

Sugden, D., D. Marchant, N. Potter, R. Souchez, G. Denton, C. Swisher III, and J. Tison (1995), Preservation of Miocene glacier ice in East Antarctica, *Nature*, *376*(6539), 412–414, doi:10.1038/376412a0.

Summerfield, M. A., F. M. Stuart, H. A. P. Cockburn, D. E. Sugden, G. H. Denton, T. Dunai, and D. R. Marchant (1999), Long-term rates of denudation in the Dry Valleys, Transantarctic Mountains, southern Victoria Land, Antarctica based on in-situ-produced cosmogenic ^{21}Ne, *Geomorphology*, *27*(1–2), 113–129.

Whitten, D., and J. Brooks (1987), *Dictionary of Geology*, Viking, New York.

G. Balco, Berkeley Geochronology Center, 2455 Ridge Road, Berkeley, CA 94709, USA.

D. Morgan, Department of Earth and Environmental Sciences, Vanderbilt University, Station B 35-1805, Nashville, TN 37235, USA. (dan.morgan@ vanderbilt.edu)

J. Putkonen, Department of Geology and Geological Engineering, University of North Dakota, Stop 8358, Grand Forks, ND 58202, USA.

J. Stone, Department of Earth and Space Sciences, University of Washington, Box 351310, Seattle, WA 98195, USA.